

## Three-dimensional simulation of oblique detonation waves attached to cone

Wenhu Han,<sup>1</sup> Cheng Wang,<sup>1,\*</sup> and Chung K. Law<sup>2,3</sup>

<sup>1</sup>*State Key Laboratory of Explosion Science and Technology, Beijing Institute of Technology, Beijing 100081, China*

<sup>2</sup>*Center for Combustion Energy, Tsinghua University, Beijing 100084, China*

<sup>3</sup>*Department of Mechanical and Aerospace Engineering, Princeton University, Princeton, New Jersey 08544, USA*



(Received 11 December 2016; published 10 May 2019)

The numerical simulation of supersonic flow over a cone is carried out to investigate oblique detonation waves. A three-dimensional (3D) conical oblique detonation wave is studied by changing the heat release. It is found that the formation of a conical oblique detonation wave shifts from a moderate transition to an abrupt transition and the frontal structure also changes from smooth to cellular features. Moreover, the conical oblique detonation wave approaches detachment as heat release increases. A comparison of oblique detonation waves attached to a 2D wedge and a 3D cone demonstrates that, for a fixed heat release, a cone is able to moderate the transition significantly, and that detaching behavior is also delayed significantly due to curvature as heat release changes. The critical heat release for detachment of the conical oblique detonation wave is much larger than that of the wedge-induced oblique detonation wave. Moreover, we assess the difference in angles of oblique detonation waves produced by wedges and cones and find that the angle is much smaller than that of wedge-induced oblique detonation wave because of flow divergence caused by the curvature (curved front in the circumference direction of the cone).

DOI: [10.1103/PhysRevFluids.4.053201](https://doi.org/10.1103/PhysRevFluids.4.053201)

### I. INTRODUCTION

Oblique detonation waves (ODWs) are attractive for hypersonic propulsion [1–7]. The concept of an ODW engine offers the potential for greater efficiency through the use of a standing ODW. A number of investigations have explored the fundamental properties of ODWs and their implementation for propulsion systems. Reviews on ODWs and their application to hypersonic propulsion were given by Shepherd [8]. Studies have been conducted for ODWs induced by wedges in simulation and experiment. Viguier, Gourara, and Desbordes [5] studied the onset of ODWs by comparing numerical and experimental results for a hydrogen-air system and observed the transition from oblique shock waves (OSW) to an ODW attached to a wedge at hypersonic speed. They used the detailed chemistry of a H<sub>2</sub>-air mixture to predict the characteristic length of OSW-to-ODW transition in experiments. Morris, Kamel, and Hanson [9] applied planar laser-induced fluorescence imaging of hydroxyl radicals (OH PLIF) and schlieren imaging to investigate shock-induced combustion phenomena in an expansion tube. In their experiments, three different modes of transition from OSW to ODW attached to the tip of a wedge were obtained for stoichiometric H<sub>2</sub>-O<sub>2</sub> mixtures with three levels of nitrogen dilution, depending on the sensitivity of the mixture. An ODW attached to a two-dimensional (2D) wedge was computed by Li, Kailasanath, and Oran [10], showing that a multidimensional detonation structure consists of a nonreactive shock in an induction

---

\*wangcheng@bit.edu.cn

zone and a set of deflagration waves, in which the shock front is closely coupled with the energy release. Choi *et al.* [11] used a high-resolution numerical simulation to observe the cell-like structure of unstable ODW attached to a wedge and indicated that the cellular structure similar to an ordinary normal detonation wave appears in the downstream field and transits from a regular to an irregular pattern. Teng *et al.* [12,13] studied numerically the unstable surface and the transition pattern of a wedge-induced ODW, proposing a criterion for determining the transition mode by simulating a 2D ODW attaching to a wedge without considering the curvature. Single-head wave or transverse waves including the left- and right-running waves on an ODW front were observed numerically for a 2D ODW attached to a wedge [14,15]. Liu *et al.* [16,17] found theoretically and numerically that a Chapman–Jouguet (CJ) oblique detonation wave (CJ ODW) plays a significant role in the structure of an ODW and explained that an attached ODW can propagate upstream. Matsuo and Fujiwara [18] numerically investigated the oscillatory instability in shock-induced combustion around a blunt body to understand the mechanism of oscillatory instability.

However, as a supersonic flow over a conical or spherical body in three dimensions, the resulting ODW differs significantly from those induced by a wedge due to diverging flow caused by the curvature effect [19]. Gilinskii and Chernyi [19] determined the critical conditions by solving for the flow in the vicinity of the body and found that wave curvature influences the process in the reaction zone and quenches the detonation. The quenching process results from the competition between chemical energy release in the region immediately behind a curved shock wave and flow expansion led by the streamline divergence in a supersonic region behind the curved shock front. Kaneshige and Shepherd [20] and Maeda *et al.* [14] studied detonation stability experimentally in terms of the curvature effect arising from the three-dimensional (3D) nature of a stabilized ODW around a projectile. Verreault and Higgins [15,21] conducted experiments into ODWs induced by hypersonic conical projectiles to investigate the initiation limits of detonation. Moreover, polar detonation was studied in wedge and axisymmetric cone configurations [21–23]. Lefebvre and Fujiwara [24] found numerically by using a detailed reaction mechanism that an ODW at low inflow Mach number would propagate upstream from its initiation location and eventually stabilize at the cone tip (prompt ODW). The difference between wedge- and cone-attached ODWs has been discussed theoretically in terms of the Rankine-Hugoniot analysis and by solving the self-similar Taylor–Maccoll flow [21]. The theoretical analysis did not consider the role of curvature on the structure of ODW attached to a cone and assumed that the ODW front was smooth and the flow between the shock front and cone surface was axisymmetric. Yang *et al.* [25] studied numerically oblique detonation wave structures induced by semi-infinite cones through 2D axisymmetric Euler equations with a one-step Arrhenius reaction kinetic model. They observed a novel formation structure of oblique detonation for the case of low incident Mach number or cone angle due to the curvature effect, with a multi-initiation point on the 2D front. However, a conical ODW is inherently 3D and the flow field between the shock and cone surface is no longer uniform, which modifies significantly the ODW features and the ODW angle as compared with the case of the wedge.

Noting that previous studies on ODW paid more attention to theoretical and numerical 2D front structure and experimental phenomena induced by a blunt body or wedge and have yet observed the 3D front structure of a conical ODW, it is of interest to investigate the 3D front structure induced by a cone. This study numerically simulates the process of supersonic flow over cone and wedge to inspect ODW structures and assess the role of curvature on ODWs. We first state the governing equations and the numerical method and then present and discuss the numerical results.

## II. GOVERNING EQUATIONS

In 3D coordinates, the compressible and reactive flow Euler equations for mass, momentum, energy, and species conservation are as follows:

$$\frac{\partial U}{\partial t} + \frac{\partial F}{\partial x} + \frac{\partial G}{\partial y} + \frac{\partial H}{\partial z} = S, \quad (1)$$

$$U = (\rho, \rho u, \rho v, \rho w, \rho E, \rho Y)^T, \quad (2)$$

$$F(U) = (\rho u, \rho u^2 + p, \rho uv, \rho uw, \rho u(E + p/\rho), \rho uY)^T, \quad (3)$$

$$G(U) = (\rho v, \rho vu, \rho v^2 + p, \rho vw, \rho v(E + p/\rho), \rho vY)^T, \quad (4)$$

$$H(U) = (\rho w, \rho wu, \rho vw, \rho w^2 + p, \rho w(E + p/\rho), \rho wY)^T, \quad (5)$$

$$S(U) = (0, 0, 0, 0, 0, \rho\omega)^T, \quad (6)$$

$$E = \frac{RT}{\gamma - 1} + YQ + \frac{1}{2}(u^2 + v^2 + w^2), \quad (7)$$

$$\omega = -KYe^{-(E_a/R_uT)}, \quad (8)$$

where  $u$ ,  $v$ , and  $w$  are the Cartesian components of fluid velocity in the  $x$ ,  $y$ , and  $z$  directions, respectively,  $\rho$  is the density,  $p$  is the pressure,  $T$  is the temperature given by the ideal gas law  $p = \rho R_u T / m$  (where  $m$  is the average molecular weight,  $R_u$  is the molar gas constant,  $K$  is the pre-exponential factor,  $E$  is the total energy per unit volume),  $Y$  is the reactant mass fraction, and  $E_a$  is the activation energy.  $Q$  is the heat of reaction per unit volume, and the specific heat ratio  $\gamma$  is 1.3, so the CJ Mach number is

$$(M_{u,CJ})^2 = 1 + Q(\gamma^2 - 1)/\gamma \left\{ 1 + \left[ 1 + \frac{2\gamma}{(\gamma^2 - 1)Q} \right]^{1/2} \right\}, \quad (9)$$

and the overdriven factor in the direction normal to the ODW front can be defined as

$$f_n = \left( \frac{M_u \sin \beta}{M_{u,CJ}} \right)^2. \quad (10)$$

The aforementioned physical quantities are dimensionless with the initial state of the homogeneous gas mixture and therefore the initial density, pressure, and temperature all equal to unity. The equations are made dimensionless based on the state of the unburned gas, as follows:

$$\begin{aligned} \bar{\rho} &= \frac{\rho}{\rho_0}, & \bar{p} &= \frac{p}{p_0}, & \bar{T} &= \frac{T}{T_0}, & \bar{u} &= \frac{u}{u_0}, & \bar{v} &= \frac{v}{u_0}, & \bar{w} &= \frac{w}{u_0}, & \bar{x} &= \frac{x}{l_{1/2}}, & \bar{t} &= \frac{t}{t_0}, \\ \bar{E} &= \frac{E}{p_0}, & \bar{K} &= \frac{K l_{1/2}}{u_0}, & \bar{Q} &= \frac{Q}{u_0^2}, & \bar{E}_a &= \frac{E_a}{R_u T_0}, \end{aligned}$$

where  $u_0 = \sqrt{R_u T_0}$  and  $t = l_{1/2}/u_0$ . The reference length  $l_{1/2}$  is the half-reaction length. Because of the self-similarity of the Euler equations, the dimensionless form and its original form are identical except that the reaction rate becomes  $\omega = -KY \exp(-E_a/T)$ . For simplicity of presentation, the overbars on the variables are dropped in the following sections. Dimensional and non-dimensional model parameters are given in Table I.

### III. NUMERICAL SPECIFICATIONS

A rectangular domain is considered over a wedge with dimensionless sizes of  $1.5 \times 1.0$ , and a cubic computational domain covers a cone with a dimensionless size of  $1.5 \times 1.5 \times 1.5$ . We simulate ODWs by changing the heat release for a fixed cone or wedge angle. In the simulation, heat release is taken as 429.3, 858.6, 1287.9, 1717.2, 2146.5, 2404.1, and 2575.8 kJ/kg, and the corresponding dimensionless  $Q = 5, 10, 15, 20, 25, 28$ , and 30, respectively. The half-reaction length  $l_{1/2}$  is defined as the distance from the shock front to half of the mass fraction in the steady ZND structure. The dimensional half-reaction lengths are  $6.4 \times 10^{-5}$ ,  $3.2 \times 10^{-5}$ ,  $1.4 \times 10^{-5}$ ,

TABLE I. Dimensional and non-dimensional fluid properties and model parameters.

Dimensional properties		Non-dimensional model parameters	
$\gamma$	1.3	$\gamma$	1.3
$p_0$	1 atm	$p_0$	1
$T_0$	300 K	$T_0$	1
$E_a/R_u$	6000 K	$E_a/R_u T_0$	20
$R_u$	8.314 J/K mol		
$m$	0.029 kg/mol		
$Q$	429.3, 858.6, 1287.9, 1717.2 2146.5, 2404.1, 2575.8 kJ/kg	$Q/R_u T_0 m$	5, 10, 15, 20, 25, 28 30
$D_{CJ}$	769.7, 1780, 1821.4, 1539.4, 1721.1, 1821.4, 1885 m/s	$D_{CJ}$	2.6, 3.7, 4.6, 5.3, 5.9, 6.2, 6.4

$8.5 \times 10^{-6}$ , and  $5.9 \times 10^{-6}$  m for 858.6, 1287.9, 1717.2, 2146.5, and 2575.8 kJ/kg, respectively, as shown in Fig. 1(a). We select the dimensional half-reaction length with  $Q = 858.6$  kJ/kg to make the pre-exponential factor dimensionless. The pre-exponential factor is adjusted to shorten a detonation structure so that the computational domain can accommodate several detonation cells.

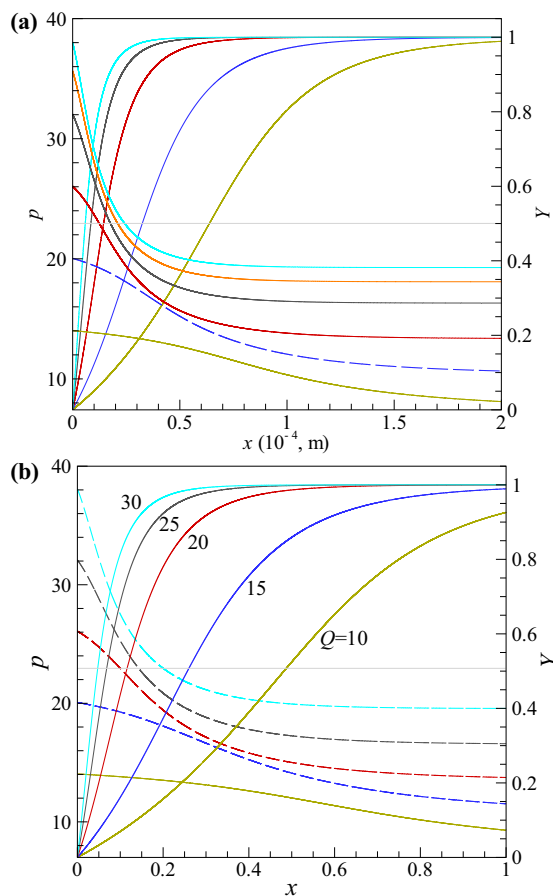


FIG. 1. Steady detonation structure for different heat releases.

Consequently, the non-dimensional half-reaction lengths are 0.5, 0.28, 0.122, 0.075, and 0.05, respectively, for  $Q = 10, 15, 20, 25,$  and  $30$ , and the corresponding grid resolutions are 200, 112, 50, 30, and 20 pts/ $l_{1/2}$  when a grid size  $\Delta x = 1/400$  is used. For a conical ODW, the curvature extends a detonation structure by lowering the heat-release rate, while the overdriven effect shortens its dimension. For a lower heat release, an ODW is more strongly overdriven. As heat release increases, the reaction zone and detonation dimension shorten. However, for an ODW, increasing the heat release reduces the overdriven factor, and consequently the mean reaction thickness approaches that of the CJ state. For  $Q = 10$ , the reaction length is  $\sim 0.5$  for steady ZND, while it reduces to approximately 0.06 for an ODW because of the strongly overdriven effect. For  $Q = 30$ , the dimension of detonation near the CJ state is about 0.2, which is much less than the domain size, with the reaction zone of about 0.05. Consequently, the dimensionless domain size of 1.5 is valid for the simulations of cases with  $Q = 10\text{--}30$ .

For a wedge-induced ODW, a wedge-surface-attached coordinate system was employed, as in previous studies [11,12]. A Mach 7 supersonic flow is used as inflow condition, and the outflow boundary is set at the right. The surfaces of wedge and cone are slip boundaries. For treating the complex wall, a fifth-order inverse Lax–Wendroff procedure [26,27] is used without violating conservation and entire resolution. We apply the fifth-order local characteristics method based on the WENO conservative finite difference scheme for space discretization and third-order TVD Runge-Kutta time discretization for time discretization [28–31]. Relative grid resolution and preserving-positivity scheme are verified for our numerical scheme so that it is able to reach the fifth order [31].

## IV. RESULTS AND DISCUSSIONS

### A. Three-dimensional conical oblique detonation waves with different heat releases

Lee [32] identified the boundary of detonation stability and observed different modes of shock oscillation through the one-dimensional simulation of detonation without curvature, showing that the oscillation mode is related to the reduced activation energy. Specifically, for  $E_a \approx 24$ , detonation is close to the neutral stability boundary and the initial oscillation is damped out for sufficiently long time. For  $E_a = 20$ , one-dimensional detonation is stable, while the detonation is two-dimensional unstable as heat release  $Q > 1.5$  and the overdrive factor  $f = 1.2$ . Although specific-heat ratio  $\gamma = 1.2$  was used in Ref. [33], the conclusion should be that any detonation wave with any finite value of  $Q$  and  $E_a$  will be unstable to transverse perturbations and develop a cellular structure [33,34]. Figure 2 shows a 3D conical ODW for different heat releases. It is seen that, for  $Q = 10$ , there is no observed cellular structure on the front of a 3D conical ODW with a moderate OSW-to-ODW transition. This is because the ODW is highly overdriven and the curvature effect also plays a role so that transversal disturbance is suppressed. For  $Q = 15$ , the cellular structure can be observed on the front, presenting the fish-scale shape shown in Fig. 2. While the transition to ODW still is smooth, it becomes more obvious than that in the case of  $Q = 10$ . For these two cases, the initiation of ODW is led by compression waves induced by an exothermic reaction. However, as heat release increases to 20, an abrupt transition to ODW is triggered by the initiating compression wave, and the cell shape becomes relatively irregular, as shown in Fig. 2(c). The cell becomes smaller and more irregular in the field far from the cone tip. Note from Figs. 2(b) and 2(c) that two humps appear in the initiation region near the cone tip before the cellular front exists, which is caused by divergence flow led by the curvature effect. Teng *et al.* [25] observed novel multi-initiation behavior that was the formation structure of oblique detonation due to the curvature effect for the axisymmetric configuration, in which the strong coupling between the shock and reaction front appeared at two distinct points. In the present simulation with a real 3D cone, the multi-initiation behavior is weakened, although the dimension of the OSW elongates significantly compared with that attached to a wedge. The difference is because of the parameters, including the specific-heat ratio, the activation energy, and the heat release, different from those in Ref. [25] and attributed partially to the 3D structure of a conical ODW.

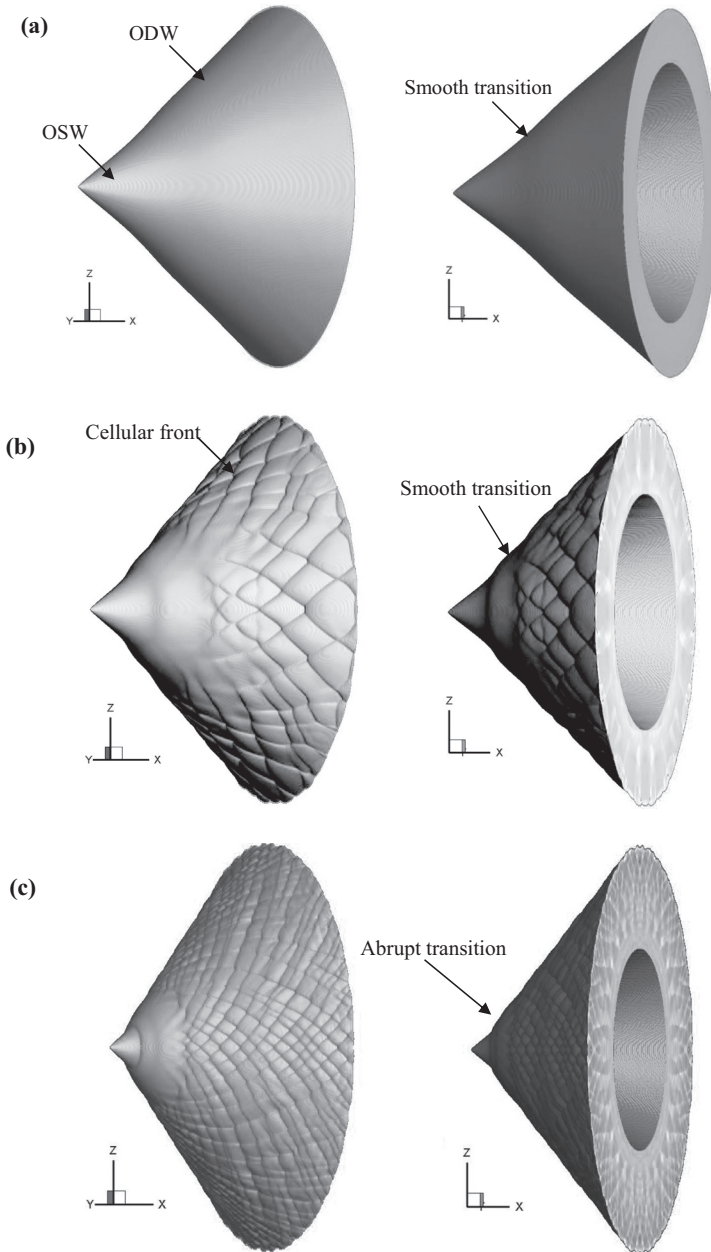


FIG. 2. 3D conical oblique detonation for (a)  $Q = 10$ , (b) 15, and (c) 20: oblique detonation wave (ODW), oblique shock wave (OSW).

As  $Q = 25$ , the transition to the ODW continues to take on the mode of prompt detonation, while the location of the transition shifts to the tip of the cone and the cell size reduces further, as shown in Fig. 3(a). This prompt ODW was observed in the experiments of Verreault and Higgins [15]. For  $Q = 30$ , the ODW almost stands at the tip of the cone and dense triple points are present at the front, demonstrating that the behavior approaches that of detaching from a cone; see Fig. 3(b).

Figure 4 shows the characteristics in an  $x$ - $z$ -plane slice for different heat releases. It is seen that the OSW-to-ODW transition and the detonation angle depend strongly on heat release. For the

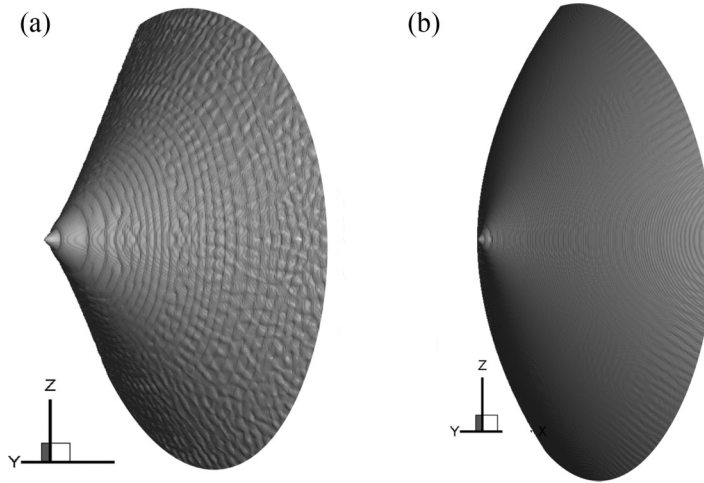


FIG. 3. 3D conical oblique detonation for (a)  $Q = 25$  and (b)  $30$ .

lower heat release of  $Q = 10$ , a smooth transition from OSW to ODW is observed at  $x \approx 0.5$  and the ODW front has no cellular structure, as shown in Fig. 4(a). While this resembles that of a 2D wedge-induced ODW in which curvature is not considered, the transition is not obvious, and its position is delayed. For  $Q = 15$ , while the OSW-to-ODW transition is still smooth, the transition point (at  $x \approx 0.4$ ) shifts toward the cone tip. For  $Q = 20$ , the abrupt transition is at  $x \approx 0.22$ , and the number of triple points increases obviously compared with that for the case of  $Q = 15$ . A shock wave, generated at the primary triple point and reflected from the cone surface, interacts with the ODW. Choi and Kim [11] observed in the 2D wedge ODW that the interaction of the reflected shock with the front initiates an ODW instability and thereby induces the frontal structure in the upstream. However, interactions of the reflected waves are weakened significantly due to transverse instability in the 3D conical ODW. The cellular instability on the conical front generally grows due to the development of the disturbances in the flow field [11]. A series of reflected waves are observed in the far field from the cone tip. The interaction of the reflected wave with transverse waves leads to a complicated pressure field, shown in Fig. 4(c). For  $Q = 25$ , the transition further moves to the tip and the number of triple points on the front increases. The transverse waves become very weak, while the reflected waves superposition into a secondary shock following behind the front; see Fig. 4(d). For  $Q = 28$ , the OSW region is very short since the transition shifts further to the cone tip. The triple point becomes very dense on the front. The reflected wave is weaker than that in the cases with  $Q = 15, 20$ , and  $25$  and also converges into a secondary shock; see Fig. 4(e). As heat release increases to  $30$ , there is no obvious inert induction zone, and the reflected waves just appear in the field near the cone tip. This indicates that the conical ODW is no longer controlled by the cone. Previous studies of ODW attached to a 2D wedge found the shift from the smooth to the abrupt OSW-to-ODW transitions [11] and developed a criterion for the transition mode [12]. However, the effect of curvature on OSW-to-ODW transitions in the conical ODW has not been assessed.

In summary, conical ODW takes on a shift from the smooth to abrupt OSW-to-ODW transition and the frontal structure varies from the smooth to the diverging cell as the heat release increases.

Close inspection of the cellular structure shows that each cell contains four nodes and curved lines; its surface transits from the convex to the concave along the longitudinal direction of ODW front. Figure 5(a) shows the triple-point line (TPL) through pressure and vorticity iso-surfaces for the case with  $Q = 15$ . At the transition point, a strong shock initiates an ODW; see the zoom-in in Fig. 5(a). A strong triple point forms at the intersection of TPLs. From the vorticity iso-surface

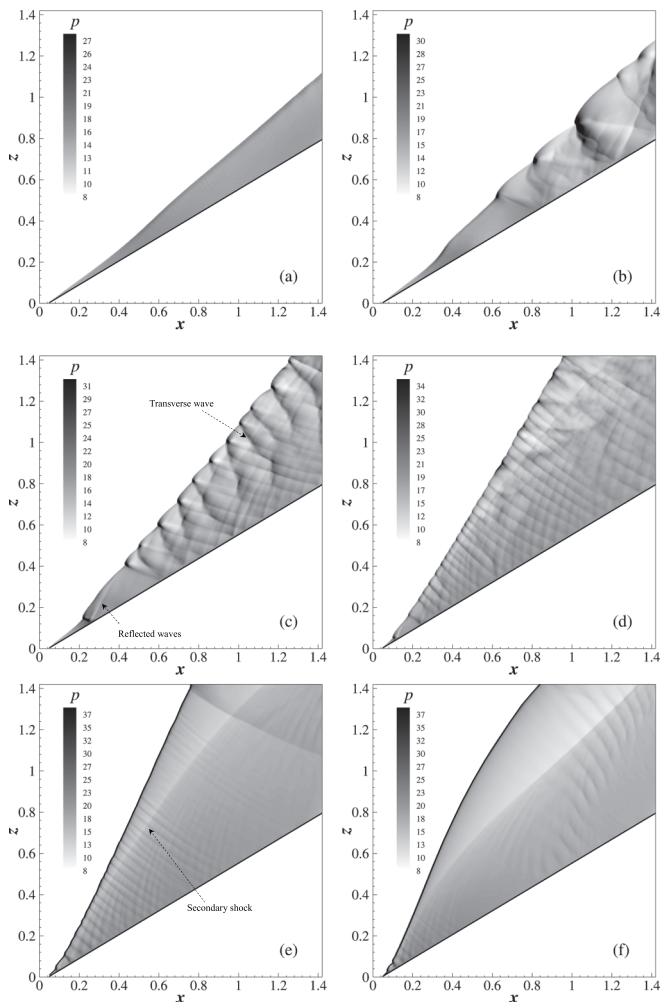


FIG. 4. Characteristics in  $x$ - $z$ -plane slice for different heat releases: (a)  $Q = 10$ , (b)  $Q = 15$ , (c)  $Q = 20$ , (d)  $Q = 25$ , (e)  $Q = 28$ , (f)  $Q = 30$ .

shown in Fig. 5(b), we observe that the entropy-vortex appears behind the strong triple points. A strong vortex tightly follows the triple points and thus extends downstream to form a pair of vortex pipes, as shown in Fig. 5(b). It is further seen that the flow behind the intersection point is not parallel to the conical surface due to the curvature effect. Moreover, corresponding to the resulting entropy vortex, the main reaction heat also generates behind the strong triples point, as shown in Fig. 5(b). However, as the Mach wave transits to the incident wave, the rate of heat release decreases, demonstrating that the cell pattern is a result of the interaction of the heat release with the entropy-vortex generated at the curved shock.

### B. Comparison of wedge- and cone-induced oblique detonation waves

Figure 6 shows an ODW attached to a 2D wedge and the characteristics in an  $x$ - $z$ -plane slice for  $Q = 10$ . It is seen that the leading shock attached to a cone is weaker than that produced by a wedge. The wedge-induced ODW has a smooth and thin front structure, resembling the studies of Choi *et al.* [11]; while in the conical 3D ODW the frontal structure on average is elongated, although

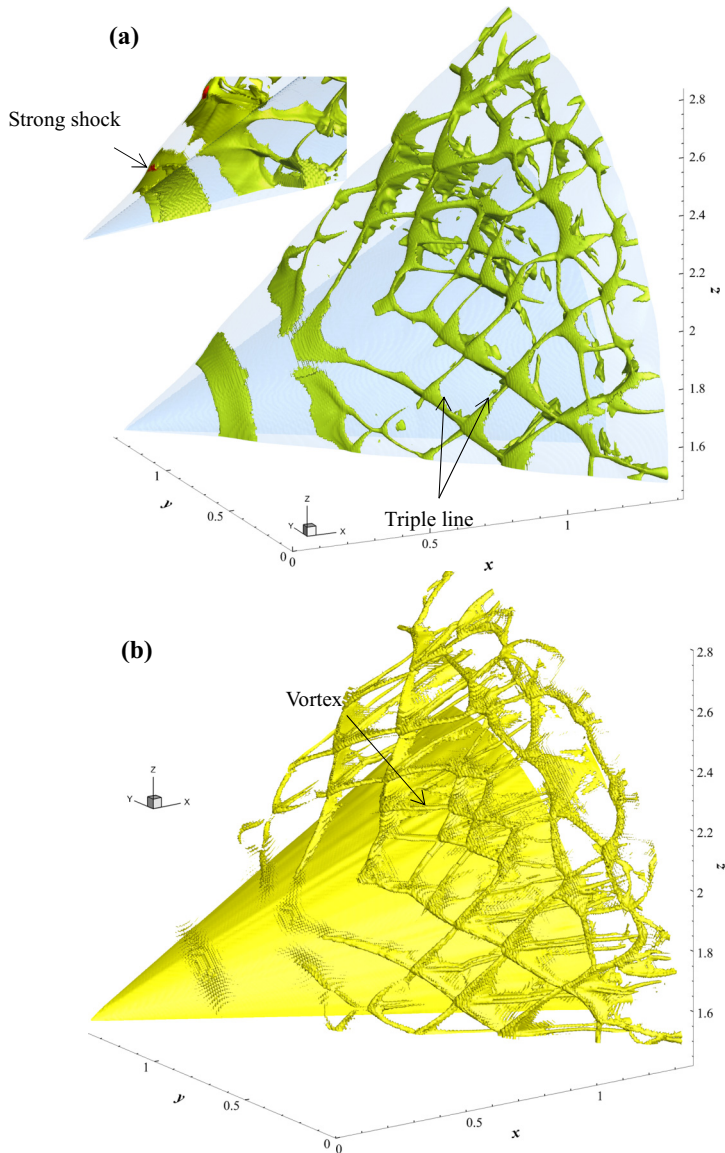


FIG. 5. Frontal structure for conical detonation wave: (a) iso-surfaces of  $p = 7.2$  for the front and  $p = 10.1$ , 20.2 for post shock; (b) iso-surfaces of vorticity = 98 and 130.

the front also is smooth; see Fig. 6(a). For  $Q = 15$ , both wedge- and cone-induced ODWs take on a cellular front structure, while their characteristics are significantly different; see Fig. 6(b). In the wedge-induced ODW, many heads appear on the front and can be divided coarsely into two types: the cell-like pattern with transverse waves behind the ODW and the normal cell in the downstream region. However, for the conical 3D ODW the number of heads on the front decreases significantly, and only the cell-like pattern remains because the detonation structure is elongated considerably due to curvature effect. For  $Q = 15$ , the wedge-induced ODW detaches from the wedge, while the conical ODW remains attached to the cone. The triple point on the front of the conical ODW is less, and the induction zone is longer compared with that in the wedge-induced 2D ODW. Therefore,

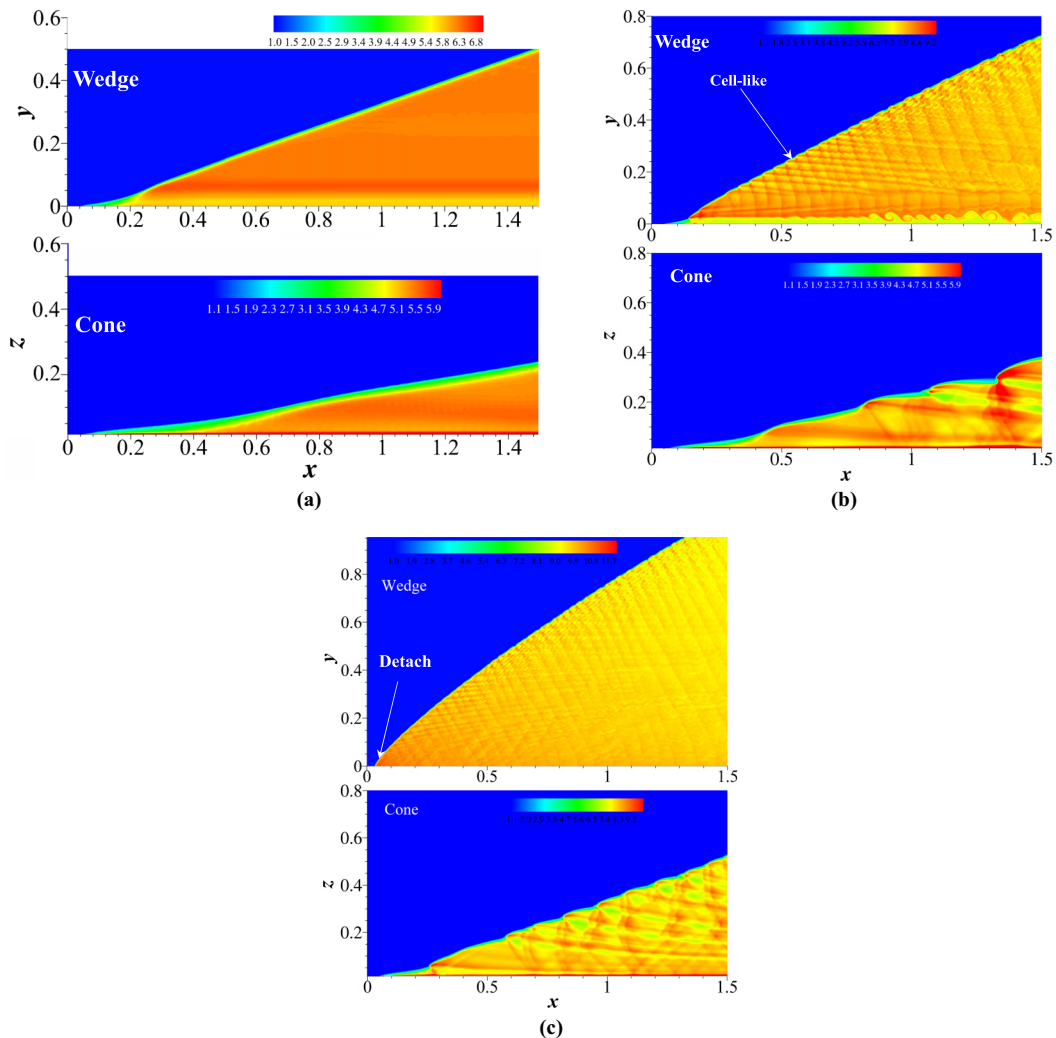


FIG. 6. Temperature contours of ODWs: the upper panel is a 2D-wedge ODW, while the lower panel is the  $x$ - $z$ -plane slice of a conical ODW which is obtained through coordinate transformation in order to compare with the wedge-induced ODW (a)  $Q = 10$ , (b)  $Q = 15$ , and (c)  $Q = 20$ .

there exists a critical heat release between  $Q = 15$  and 20 to detach the ODW from a wedge, which agrees with that predicted by the theoretical solution in Fig. 6.

It is clearly known that a curved detonation front always produces the divergence of flow behind its front. One can understand this from the fact that curvature or loss from the divergent flow reduces the detonation velocity or post-shock temperature  $T_s$ . Indeed, we observe from Fig. 6 that the post-shock temperature in the cone-induced ODW is obviously lower than that in the wedge-induced ODW. The leading-order effect increases the effective activation energy, owing to the drop in post-shock temperature. Consequently, the increase of effective activation energy  $E_a/RT_s$  in the one-step overall model makes induction time longer and leads to the extension of the detonation dimension, as shown in Fig. 7. Therefore, we expect to see the reduction of the number of wave heads on the front and the increase of OSW region compared with the wedge-induced ODW. This also explains why the conical ODW differs significantly from the wedge-induced 2D ODW. The comparison

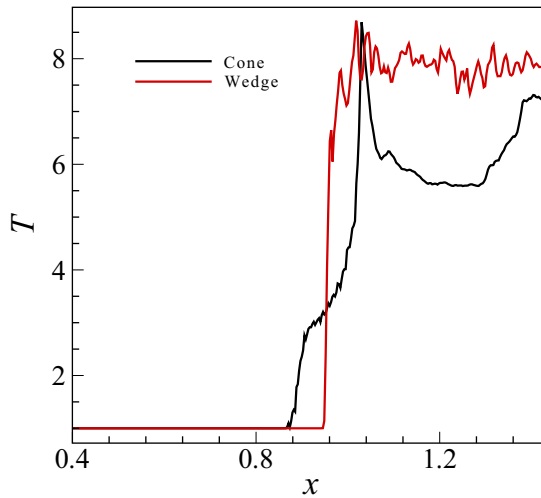


FIG. 7. Temperature profiles along the cut of  $x = 0.9$  for  $Q = 15$ .

between the results of wedge and cone in Fig. 7 indicates that the temperature near the cone surface is higher than that near the wedge by about 30% because of the effect of the Taylor–Maccoll flow, which has been substantiated in Refs. [15,25]. Furthermore, the ratio of the induction length for the cone to that for the wedge is  $\sim 3.1$  for  $Q = 10$  and  $\sim 3.76$  for  $Q = 15$ .

Figure 8 shows a plot of ODW angle vs heat release for a 2D wedge. The theoretical solution shows a dual solution, turning point behavior of the inverse C-shape curve, demonstrating that a detaching behavior can appear as the strong overdriven ODW transits to the weak overdriven ODW. It is known further that the detaching angle is  $66.5^\circ$  at the critical heat release of  $\sim 18$ , which is comparable to that predicted by a simulation of the wedge-induced ODW. The angle of ODW attached to the 2D wedge is consistent with the theoretical solution, while the conical ODW angle is significantly lower than the theoretical and numerical solutions. In the present simulations, for

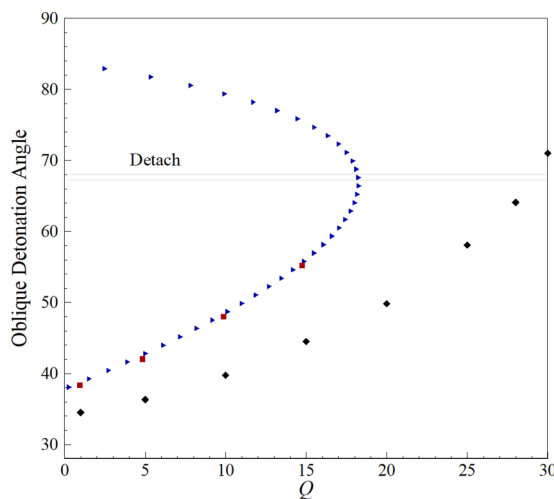


FIG. 8. Curve of oblique detonation angle vs heat release: blue dots are theoretical solution without the curvature; black dots are for ODW attached to cone; red squares are for ODW attaching to a wedge.

TABLE II. Overdriven factors for different heat release.

Case	$f_n$
$Q = 10$	3.86
$Q = 15$	2.78
$Q = 20$	2.12
$Q = 25$	1.66
$Q = 28$	1.35
$Q = 30$	1.06

$Q = 10$  the OSW and ODW angles for the conical ODW are respectively 36.1 and 39.8, which are close to that obtained by Verreault and Higgins [21]. This difference between the angles of wedge- and cone-induced ODWs is 6.0° for  $Q = 15$  and 9.8° for  $Q = 20$ . The angle for  $Q = 15$  is theoretically 51.4° [11], which is larger than that calculated in the simulations of the conical ODW. Moreover, the angle difference is lower than that in Ref. [11] and almost increases linearly with increase in heat release. This is reasonable because the curvature lowers the angle and increases the critical heat release for the detachment. The trend agrees with that measured in experiments and the predicted values are lower than that measured in the experiments of Verreault and Higgins [15]. They suggested that the discrepancy was most likely caused by unsteady effects or curvature effects of the detonation front. Indeed, the above discussions are able to validate the curvature effect on this discrepancy. For  $Q = 30$  the conical ODW transits to a weak overdriven regime, while it approaches the detachment, but does not detach from the cone. Consequently, the detaching behavior is significantly delayed due to the divergence of flow led by the curvature of the cone surface, compared with that induced by the wedge. Li and Kailasanath [10] explained the detachment of a 2D ODW from a wedge by changing the Mach number. They found that the flow in the transition region from the subsonic to the supersonic was critical for maintaining the ODW structure attached to the wedge. Our results show that, as heat release increases, the normalizing overdriven factor  $f_n$  decreases; see Table II. For  $Q = 10$ ,  $f_n$  is 3.86 and relatively strong overdriven suppresses the development of the instability. This also is partially the reason for the smooth conical front of the 3D ODW with  $Q = 10$ . As  $Q$  increases,  $f_n$  decreases, demonstrating that the overdriven degree in the normal direction weakens. For all cases of  $Q = 10, 15,$  and  $20$ , totally the Mach number behind the front is larger than unity, and the flow here is supersonic, as shown in Fig. 8. As  $Q$  increases further,  $f_n$  decreases and the ODW is apt to detach from the cone.

In summary, for a 3D conical ODW, the extended structure leads to the reduction of reaction rate and consequently detonation angle due to the curvature effect. Consequently, while the wedge-induced ODW has the agreement of the detonation angle with the corresponding detonation polar, the angle of a conical ODW is lower than that induced by a wedge. The 3D cone makes detaching behavior more difficult, leading to a larger critical heat release for detachment than that of 2D ODW attached to a wedge.

### C. Verification of grid convergence

We simulated the 2D ODW attached to a wedge with three levels of  $\Delta x = 1/200, 1/400,$  and  $1/800$  to identify grid convergence for the case with  $E_a = 15$  and the wedge angle of 30°. Figure 9 shows that, as the grid resolution increases to  $1/800$ , the cell structure and detonation angle are not affected significantly by the grid resolution, demonstrating that the result obtained with  $\Delta x = 1/400$  converges to that obtained with  $\Delta x = 1/800$ . Hence, the grid resolution of  $\Delta x = 1/400$  is enough to capture the ODW front structure and predict the ODW angle. Choi and Kim *et al.* [11] used a third-order MUSCL-type TVD scheme to discretize the convective fluxes and identified that the results obtained with the grid resolution of  $\Delta x = 1/500$  can converge well to those obtained with  $\Delta x = 1/1000$  and  $1/2000$  for the case of  $E_a = 20$  and  $Q = 10$ . However, the present simulations

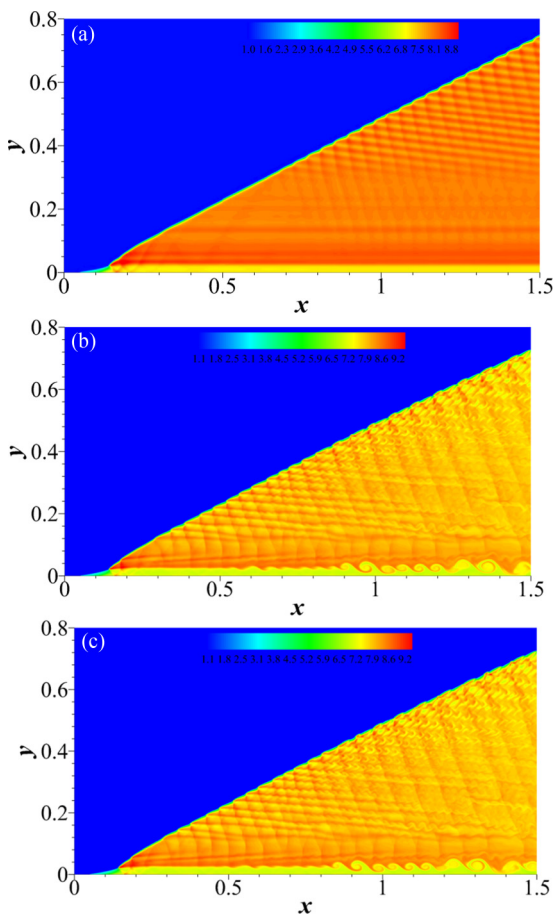


FIG. 9. Verification of grid-resolution convergence of 2D ODW attached to a wedge.

used a fifth-order WENO scheme and thereby relatively less grid can reach a higher resolution. Its accuracy has been verified and can indeed reach the fifth order for a 3D detonation [31,35]. For higher grid resolution, strong vorticity generation occurs at the contact surface, which was discussed in more detail by Choi *et al.* [11]. In the present simulation, physical viscosity is not considered so that small-scale vortices observed by Mazaheri *et al.* [36] do not appear. The vorticity generated on the contact surface in Figs. 9(b) and 9(c) is caused by Kelvin–Helmholtz instability from the primary triple point.

For the ODW induced by a cone, the leading shock strength can be weakened by the diverging flow effect of the curved cone surface. Yang *et al.* [25] demonstrated that the average heat release rate was lower than that of the traditional structure and was illustrated by the enlarged thickness of the heat-release layer. Consequently, the dimension of the detonation structure is longer than that of the wedge-induced ODW. The grid resolution of  $\Delta x = 1/400$  should be valid for simulations of a conical 3D ODW. To identify further the grid convergence, we simulated a conical 3D ODW with three levels of  $\Delta x = 1/200$ ,  $1/400$ , and  $1/800$  for the case with  $E_a = 15$ . For  $\Delta x = 1/200$ , the main characteristics of the conical 3D ODW can be captured and the cell structure is regular, while the flow field between the shock front and the cone surface is not described well and the OSW-to-ODW transition is blurry; see Fig. 10(a). As grid resolution increases, the frontal cells become irregular and the OSW-to-ODW transition is clearer, as shown in Figs. 10(b) and 10(c). The frontal structure of ODW obtained with  $\Delta x = 1/400$  converges to that with  $\Delta x = 1/800$ ,

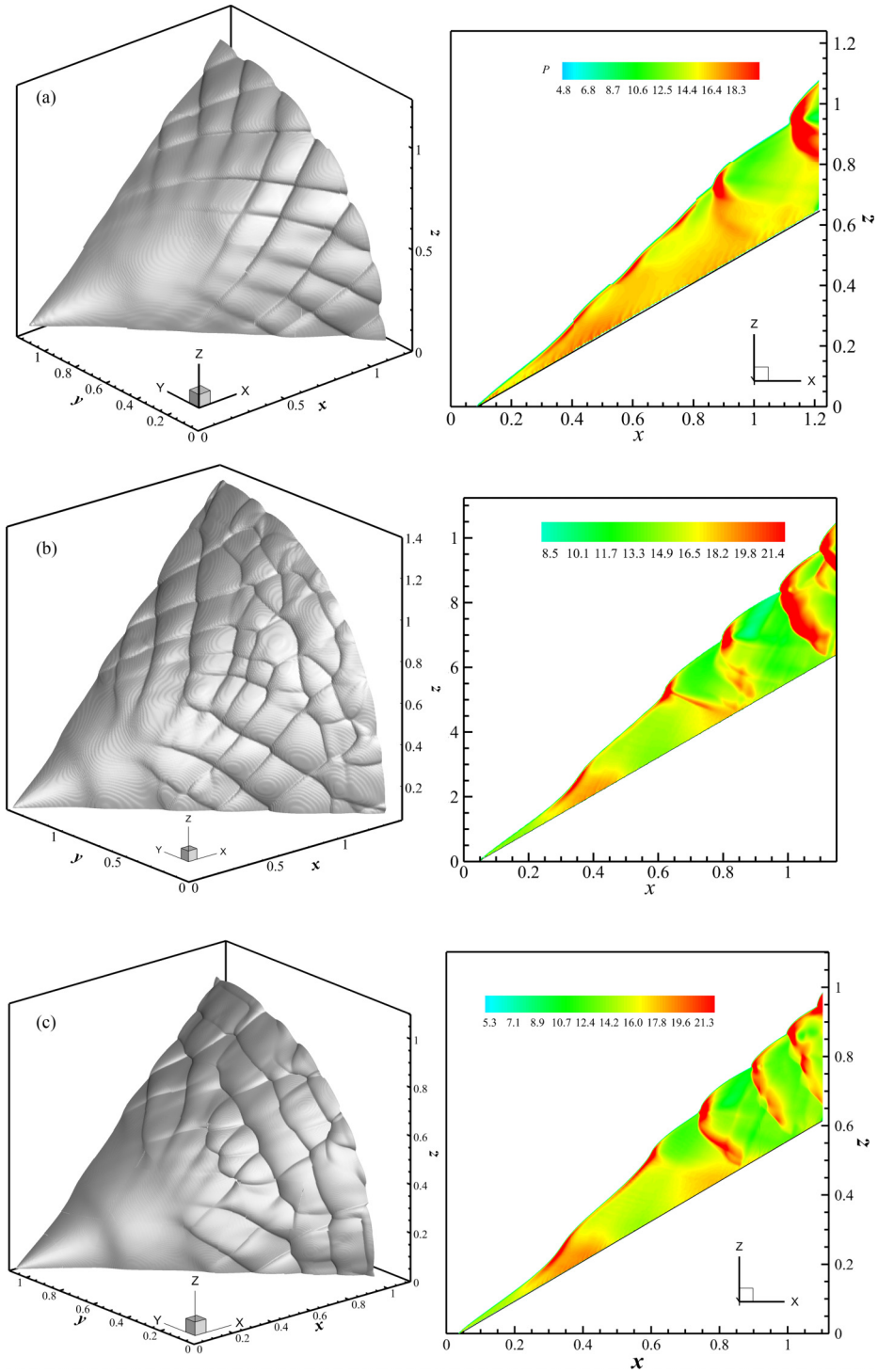


FIG. 10. Verification of grid-resolution convergence for cone-induced 3D ODW with  $Q = 15$ : (a)  $\Delta x = 1/200$ , (b)  $\Delta x = 1/400$ , (c)  $\Delta x = 1/800$ . The upper panel shows the three-dimensional front structure, while the lower panel shows slices in the  $x$ - $z$  plane of  $y = 0.5$ .

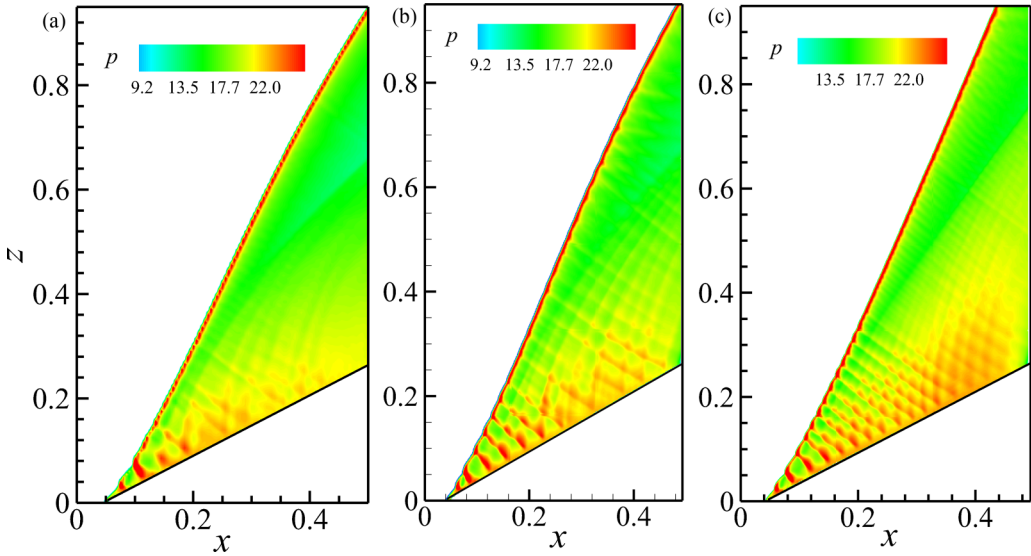


FIG. 11. Verification of grid-resolution convergence for cone-induced 3D ODW with  $Q = 30$ : (a)  $\Delta x = 1/400$  (20 pts/ $L_{1/2}$ ), (b)  $\Delta x = 1/600$  (30 pts/ $L_{1/2}$ ), (c)  $\Delta x = 1/800$  (40 pts/ $L_{1/2}$ ). Slices are in the  $x$ - $z$  plane.

demonstrating that a grid convergence is achieved. For the heat release of  $Q = 30$ , the higher level of grid resolution is required to capture the frontal structure of 3D conical ODW. The heat release of  $Q = 30$  is selected to carry out the simulations with two levels of  $\Delta x = 1/400$  and  $1/800$ . Figure 11 shows that global characteristics are still comparable for these two grid resolutions, although a minor difference downstream is also observed. It is seen that refining cell size does not change the ODW angle and detaching behavior, while it just leads to finer cellular structure observed on the front, as shown in Fig. 11(b). Therefore, the present grid resolution is valid for the prediction of a conical ODW angle for  $Q = 30$ .

Next, the validation of the present grid resolution is identified quantitatively. For  $Q = 15$ , the pressure profiles are extracted from the  $x$ - $z$  slice of results obtained with 50 and 100 pts/ $L_{1/2}$  (Fig. 10), which are along cuts parallel to the cone surface at  $z = 0.0$  and  $0.1$ , respectively, shown in Fig. 12. It is seen that the pressure profiles obtained with 50 and 100 pts/ $L_{1/2}$  are globally consistent, with minor differences. This indicates that the present grid resolution is enough to capture the global structure of ODW for  $Q = 15$ .

Figure 13 shows pressure profiles along cuts ( $z = 0.0$  and  $z = 0.2$  in Fig. 11) parallel to the cone wall for  $Q = 30$ . We observe that, for these two grid resolutions, pressure profiles have global agreement, while disparity downstream presents locally. Furthermore, the detonation angles and the global structures tend to be consistent for 20, 30, and 40 pts/ $L_{1/2}$ . The structures on the ODW front do not disappear with the increase of grid resolution, showing that they are not numerical noise. Figure 13 shows quantitatively that increasing the grid resolution does not change the ODW angle, although the structure on the front and flow downstream change slightly. Consequently, for  $Q = 30$ , the present grid resolution is valid to assess the role of curvature in the ODW attached to a cone and to describe global characteristics. Nevertheless, the present grid resolution may be insufficient to capture finer structures at the surface of the ODW with  $Q = 30$ , and a finer cellular structure requires a higher grid resolution.

In summary, for the Euler system, there is no explicit physical viscosity to be introduced as a cutoff length scale below which physical viscosity starts to work so that the numerical results vary slightly with the increase of grid resolution. In the present simulation, the grid resolution can capture the global feature of ODW and predict the ODW angle for all cases, although for a large

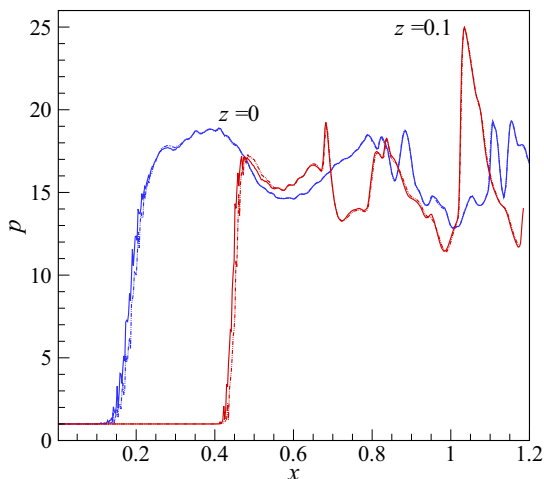


FIG. 12. Pressure profiles along cuts ( $z = 0$  and  $0.1$ ) parallel to the cone wall for  $Q = 15$ : solid (50 pts/ $L_{1/2}$ ), dashed line (100 pts/ $L_{1/2}$ ).

heat release the finer structures slightly change with increasing grid resolution. Furthermore, for  $Q = 30$  the resolution of 20 pts/ $L_{1/2}$  is relatively lower, compared with 128 pts/ $L_{1/2}$  in Teng *et al.* [25]. Nevertheless, the present numerical simulation used a fifth-order WENO scheme that utilized relatively fewer grids to reach a higher resolution. Due to curvature effects, the heat release rate in the detonation structure is weakened and the reaction length is extended, so the grid resolution for  $Q = 30$  is still valid. Nevertheless, the grid resolution is insufficient for capturing finer structures of ODW with  $Q = 30$ , which requires a higher grid resolution. Since the study focuses mainly on the effect of curvature on the global feature and ODW angle, the numerical solution for  $Q = 30$  is still reliable.

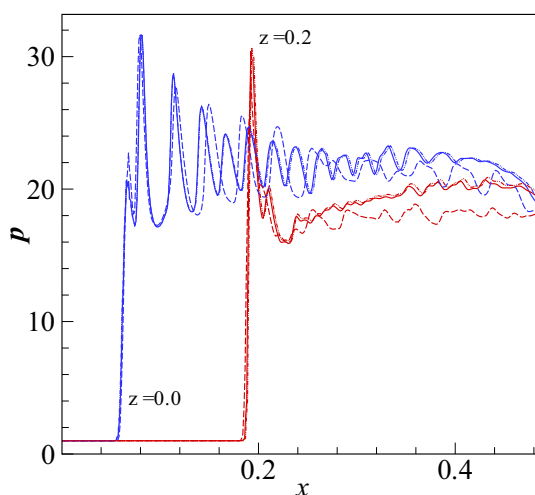


FIG. 13. Pressure profiles along cuts ( $z = 0.0$  and  $0.2$ ) parallel to the cone surface for the case with  $Q = 30$ : dashed line ( $\Delta x = 1/400$ , 20 pts/ $L_{1/2}$ ), solid ( $\Delta x = 1/600$ , 30 pts/ $L_{1/2}$ ), and dot-dot-dashed ( $\Delta x = 1/800$ , 40 pts/ $L_{1/2}$ ).

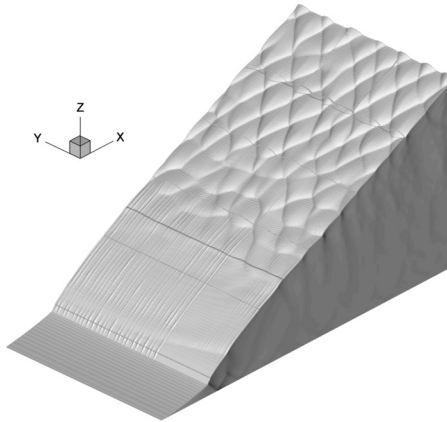


FIG. 14. Frontal structure of wedge-induced 3D ODW for  $Q = 15$ .

**D. Effect of dimensions on oblique detonation waves attached to a wedge**

We chose the case with  $Q = 15$  to simulate an ODW attached to 3D wedge and identify the effect of dimensions on ODW angle. Figure 14 shows that the ODW front takes on cell structure; the cells are relatively regular. While the cell shape is similar to the fish scale formed by temporal and spatial evolution of triple points in 2D channels, it is of 3D characteristics in the third direction. The slice of the  $x$ - $z$  plane is extracted to compare with the 2D ODW. There are similar features between wedge-induced 2D and 3D ODWs, as shown in Fig. 15. The measured detonation angle of the wedge-induced 3D ODW is equal to that in the corresponding 2D case; the dimension of 3D ODW front structure is equal to that of the 2D ODW.

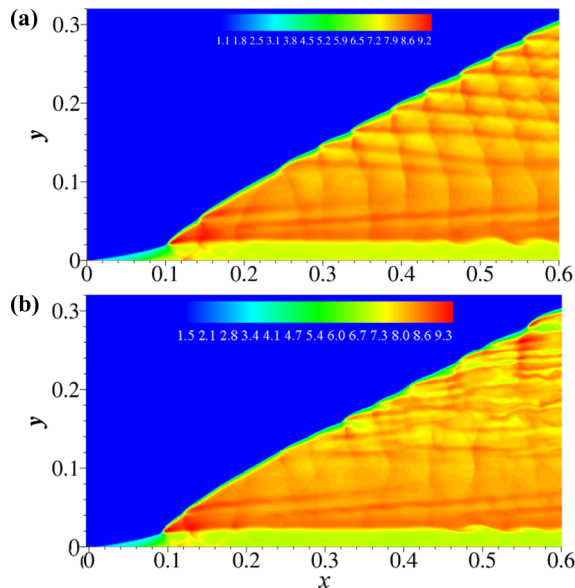


FIG. 15. Characteristics in cuts of ODWs attached to (a) 2D and (b) 3D wedges for  $Q = 15$ .

## V. CONCLUSIONS

The 3D conical ODW has been presented clearly by performing a high-resolution numerical simulation. It is found that the conical ODW takes on the transition from the smooth to the cellular front as heat release increases. This cellular conical ODW is capable of swallowing much more fuel, with a rapid output of huge energy, and maintaining an excellent stationary state, and thereby will become a very promising combustion mode for some supersonic propellers. Conical ODWs take on a shift from the smooth to abrupt OSW-to-ODW transition with a change in the heat release. Moreover, as the overdriven factor decreases and approaches unity, the conical ODW approaches detachment from the cone.

Comparison of cone- and wedge-induced ODWs shows that the ODW angle for the cone is much smaller than that induced by the wedge due to the curvature of the cone surface. It is found that the cone is able to moderate and delay the occurrence of the OSW-to-ODW transition, compared with the wedge.

## ACKNOWLEDGMENTS

This research was supported by the National Natural Science Foundation of China (Grants No. 11732003, No. 91541206, and No. 11572258), the Beijing Natural Science Foundation (Grant No. 8182050), the Science Challenge Project (Grant No. TZ2016001), and the National Key R&D Program of China (Grant No. 2017YFC0804700).

- 
- [1] R. Dunlap, R. L. Brehm, and J. A. Nicholls, A preliminary study of the application of steady-state detonative combustion to a reaction engine, *Jet Propul.* **28**, 451 (1958).
  - [2] A. Hertzberg, A. P. Bruckner, and D. W. Bogdanoff, Ram accelerator - a new chemical method for accelerating projectiles to ultrahigh velocities, *AIAA J.* **26**, 195 (1988).
  - [3] M. J. Grismer and J. M. Powers, Numerical predictions of oblique detonation stability boundaries, *Shock Waves* **6**, 147 (1996).
  - [4] R. C. Viguier, S. L. Figueira da, D. Desbordes, and B. Deshaies, Onset of oblique detonation waves: comparison between experimental and numerical results for hydrogen-air mixtures, *Proc. Combust. Inst.* **26**, 3023 (1997).
  - [5] C. Viguier, A. Gourara, and D. Desbordes, Three-dimensional structure of stabilization of oblique detonation wave in hypersonic flow, *Proc. Combust. Inst.* **27**, 2207 (1998).
  - [6] S. L. Figueira da and B. Deshaies, Stabilization of an oblique detonation wave by a wedge: A parametric numerical study, *Combust. Flame* **121**, 152 (2000).
  - [7] J. Kasahara, T. Fujiwara, T. Endo, and T. Arai, Chapman–Jouguet oblique detonation structure around hypersonic projectiles, *AIAA J.* **39**, 1553 (2001).
  - [8] J. E. Shepherd, Detonation Waves and Propulsion, in *Combustion in High-Speed Flows*, edited by J. Buckmaster, T. L. Jackson, and A. Kumar (Kluwer Academic, Norwell, 1994), pp. 373–420.
  - [9] C. I. Morris, M. R. Kamel, and R. K. Hanson, Shock-induced combustion in high-speed wedge flows, *Proc. Combust. Inst.* **27**, 2157 (1998).
  - [10] C. Li, K. Kailasanath, and E. S. Oran, Detonation structures behind oblique shocks, *Phys. Fluids* **6**, 1600 (1994).
  - [11] J. Y. Choi, D. W. Kim, I. S. Jeung, F. Ma, and V. Yang, Cell-like structure of unstable oblique detonation wave from high-resolution numerical simulation, *Proceed. Combust. Institut.* **31**, 2473 (2007).
  - [12] H. H. Teng and Z. L. Jiang, On the transition pattern of the oblique detonation structure, *J. Fluid Mech.* **713**, 659 (2012).

- [13] H. H. Teng, Z. L. Jiang, and H. D. Ng, Numerical study on unstable surfaces of oblique detonations, *J. Fluid Mech.* **744**, 111 (2014).
- [14] S. Maeda, S. Sumiya, J. Kasahara, and A. Matsuo, Scale effect of spherical projectiles for stabilization of oblique detonation waves, *Shock Waves* **25**, 141 (2015).
- [15] J. Verreault, A. J. Higgins, and R. A. Stowe, Formation of transverse waves in oblique detonations, *Proceed. Combust. Inst.* **34**, 1913 (2013).
- [16] Y. Liu, D. Wu, S. Yao, and J. Wang, P. Analytical and numerical investigations of wedge-induced oblique detonation waves at low inflow Mach number, *Combust. Sci. Tech.* **187**, 843 (2015).
- [17] Y. Liu, Y.-S. Liu, D. Wu, and J.-P. Wang, Structure of an oblique detonation wave induced by a wedge, *Shock Waves* **26**, 161 (2016).
- [18] A. Matsuo and T. Fujiwara, Numerical investigation of oscillatory instability in shock-induced combustion around a blunt body, *AIAA J.* **31**, 1835 (1993).
- [19] S. M. Gilinskii and G. G. Chernyi, Supersonic flow of combustible gas mixture past sphere with account for ignition delay time, *Fluid Dynam.* **3**, 12 (1968).
- [20] M. J. Kaneshige and J. E. Shepherd, Oblique detonation stabilized on a hypervelocity projectile, *Proc. Combust. Inst.* **26**, 3015 (1996).
- [21] J. Verreault, A. J. Higgins, and R. A. Stowe, Formation and structure of steady oblique and conical detonation waves, *AIAA J.* **50**, 1766 (2012).
- [22] R. A. Gross, Oblique detonation waves, *AIAA J.* **1**, 1225 (1963).
- [23] D. T. Pratt, J. W. Humphrey, and D. E. Glenn, Morphology of standing oblique detonation waves, *J. Propul. Power* **7**, 837 (1991).
- [24] M. H. Lefebvre and T. Fujiwara, Numerical modeling of combustion processes induced by a supersonic conical blunt body, *Combust. Flame* **100**, 85 (1993).
- [25] Y. P. Yang, H. D. Ng, H. H. Teng, and Z. L. Jiang, Initiation structure of oblique detonation waves behind conical shocks, *Phys. Fluids* **29**, 086104 (2017).
- [26] S. R. Tan, C. Wang, C. W. Shu, and J. G. Ning, Efficient implementation of high order inverse Lax-Wendroff boundary treatment for conservation laws, *J. Comput. Phys.* **231**, 2510 (2012).
- [27] C. Wang, J. X. Ding, S. R. Tan, and W. H. Han, High order numerical simulation of detonation wave propagation through complex obstacles with the inverse Lax-Wendroff treatment, *Commun. Computat. Phys.* **18**, 1264 (2015).
- [28] G. S. Jiang and C. W. Shu, Efficient implementation of weighted ENO schemes, *J. Comput. Phys.* **126**, 202 (1996).
- [29] D. S. Balsara and C. W. Shu, Monotonicity preserving weighted essentially non-oscillatory schemes with increasingly high order of accuracy, *J. Comput. Phys.* **160**, 405 (2000).
- [30] X. Zhang and C. W. Shu, Positivity-preserving high order finite difference WENO schemes for compressible Euler equations, *J. Comput. Phys.* **231**, 2245 (2012).
- [31] C. Wang, C. W. Shu, W. H. Han, and J. G. Ning, High resolution WENO simulation of 3D detonation waves, *Combust. Flame* **160**, 447 (2013).
- [32] S. H. J. Lee, *Detonation Phenomenon* (Cambridge University, Cambridge, UK, 2008).
- [33] M. Short and D. S. Stewart, Cellular detonation stability: A normal mode linear analysis, *J. Fluid Mech.* **368**, 229 (1998).
- [34] H. D. Ng and F. Zhang, Detonation instability, *Shock Waves Sci. Technol. Library* **6**, 107 (2012).
- [35] W. Han, W. Kong, Y. Gao, and C. K. Law, The role of global curvature on the structure and propagation of weakly unstable cylindrical detonations, *J. Fluid Mech.* **813**, 458 (2017).
- [36] K. Mazaheri, Y. Mahmoud, M. Sabzpooshani, and M. Radulescu, I. Experimental and numerical investigation of propagation mechanism of gaseous detonations in channels with porous walls, *Combust. Flame* **162**, 2638 (2015).